Human-in-the-Loop Control of Robotic Leg Prostheses With Sensory Feedback

Ming Pi, Zhijun Li, *Fellow, IEEE*, Qinjian Li, Yu Kang, *Senior Member, IEEE*, Zhen Kan, *Senior Member, IEEE*, and Rong Song, *Senior Member, IEEE*

***Abstract*—Human during walking can sense the joint angle and the contact force between the leg and the ground and uses such information as the feedback to regulate walking performance. To complete this motor control for the amputee with the leg prosthesis, human-in-the-loop control was proposed. This control method involves the restoration of the sensory feedback and the unified gait generator. By restoring the sensory feedback of the prosthesis with noninvasive Functional Electrical Stimulation (nFES), the subject can sense touch-down moment, leave-off moment, and height of small obstacles on the ground. Then, the unified gait generator converts the subject's intent into the prosthesis' motor command according to the damping and Spring-Loaded Inverted Pendulum (D-SLIP) model. When walking is slow, the prosthesis is stiff. When walking is fast, the prosthesis is compliant. Three experiments were conducted to prove the improvement of walking performance, such as the precision to sense the height of small obstacles, and the amount of increment for walking speed and frequency on level ground, *S* curve, or stairs. These results showed that the proposed control method can improve the motion capability of subjects greatly.**

***Index Terms*—Human-in-the-loop control, robotic leg prostheses, sensory feedback.**

Manuscript received 21 November 2022; revised 19 May 2023; accepted 25 September 2023. Date of publication 20 October 2023; date of current version 18 June 2024. Recommended by Technical Editor P. Yan and Senior Editor K. J. Kyriakopoulos. This work was supported in part by the National Key RD Program of China under Grant 2021YFF0501600, in part by the National Natural Science Foundation of China under Grant U22A2060 and Grant 62133013, in part by the Major Science and Technology Projects of Anhui Province under Grant 202103a05020004, in part by the Anhui Provincial Natural Science Foundation under Grant 2208085UD09 and Grant 2208085QF208, and in part by the Southwest University of Science and Technology Doctoral Fund under Grant 21zx7142. *(Corresponding author: Zhijun Li.)*

This work involved human subjects or animals in its research. Approval of all ethical and experimental procedures and protocols was granted by the Ethics Committee of Yueyang Hospital of Integrated Traditional Chinese and Western Medicine, Shanghai, University of Traditional Chinese Medicine, under Application No. 2019-014, and performed in line with the approval of ethical review.

Ming Pi is with the School of Information Engineering, Southwest University of Science and Technology, Mianyang 621010, China (e-mail: piming1987@outlook.com).

Zhijun Li is with the Institute of Artificial Intelligence, Hefei Comprehensive National Science Center, Hefei 230031, China, and also with the School of Mechanical Engineering, Tongji University, Shanghai 200092, China (e-mail: zjli@ieee.org).

Qinjian Li and Zhen Kan are with the Department of Automation, University of Science and Technology of China, Hefei 230027, China (e-mail: lqj0414@mail.ustc.edu.cn; zkan@ustc.edu.cn).

Yu Kang is with the Department of Automation, Institute of Advanced Technology, University of Science and Technology of China, Hefei 230027, China (e-mail: kangduyu@ustc.edu.cn).

Rong Song is with the School of Engineering, Sun Yat-sen University, Guangzhou 510000, China (e-mail: songrong@mail.sysu.edu.cn).

Color versions of one or more figures in this article are available at https://doi.org/10.1109/TMECH.2023.3321403.

Digital Object Identifier 10.1109/TMECH.2023.3321403

I. Introduction

SENSORY feedback is essential to the motor control of the human body, the adaptation of gait movement and the corresponding stability of joint displacement, spatial understanding of the relative situation of the body, and the sensation of external force from the interaction with the environment [1], [2]. Because of the lost sensory feedback system, even if robotic leg prostheses have been used for years, there still exists a big gap between an intact leg and a robotic leg in terms of motor ability.

While applying the sensory feedback to robotic leg prostheses, two major challenges should be addressed: 1) how to restore the lost proprioceptive sensation within prosthetic systems efficiently, and 2) how to close the loop from the sensory feedback system to realize the normal human gait adaptation efficiently.

The sensory feedback is of vital importance for the fully functional motion control of the prosthesis. However, the complexity of sensory feedback systems imposes great challenges in the design of bionic prosthesis systems, which can be improved with a bidirectional communication framework via the sensory feedback. The main objective of introducing the sensory feedback in the prosthetic system is to imitate the mechanoreceptors in a natural manner and to produce the corresponding proprioceptive sensation [3], [4]. The individual kinesthetic awareness and the cutaneous touch perception could be recovered by using the techniques of direct stimulation by implanting electrodes in the upstream peripheral nerves [5]. However, due to the low accuracy and weak resolution of simulation techniques, none of these approaches can stably provide natural sensory feedback. In [6], a vibration-induced illusory was proposed for the perceptual characteristics of a sense of a force induced by asymmetric vibration using a vibration-speaker-type nongrounded haptic interface.

Nevertheless, the practice of this sensory feedback approach is challenging. The feasibility of controlling myoelectric prostheses can be improved using the target muscle reinnervation in an efficient way [7]. However, such an approach is not designed for closed control loops with proprioceptive sensation. To address these challenges, one of the promising solutions is regenerative

peripheral nerve interfaces [8]. However, the neurosurgical procedure is not affordable to most practical patients, and its safety issue is also challenging for clinical application because placing electrodes in the nerves can potentially damage the nerve system of patients.

A practical alternative to nerve implants could be stimulated by noninvasive electrodes, which do not need surgery for chronic implants [9]. Functional electrical stimulation (FES) has many benefits, such as fast application and accurate modulation, since the stimulation parameters can be freely controlled [10]. Information can be transmitted by means of parameter modulation or spatial coding [11]. In the electrical stimulation, the electric current passes through the skin and evokes sensations by activating cutaneous sensory fibers or receptors [3].

In [9], FES was proposed to establish the sensory feedback, to help the subject perceive the movement of the prosthetic leg. However, the use of FES is not considered in the control design, and few insightful analyses is included. Particularly, this work is different from that in [9] in the following aspects: 1) FES in this current work can adjust the motion impedance characteristics of the prosthetic leg, leading to a complete closed-loop control of the prosthetic leg to sense the height of small obstacles; 2) the experiments in this current work have been conducted and verified on the lower limb amputees.

FES has been used for the control of the lower extremity. FES combined with the motor-imagery-based brain–computer interface has been studied for the improvement of patients' motor function in neuro-rehabilitation and motor assistance. FES has been used to stimulate the subjects' lower limbs before their imagination of the muscles' contraction and improve their attention on the lower limbs [12]. Moreover, the movements induced by FES tend more toward active movement instead of the passive movement, by comparing the event-related desynchronization patterns during active movement, passive movement, and FES-induced movement of the lower limb [13]. Although the noninvasive sensory feedback is also promising for the future of robotic leg prostheses, integrating this information in a human-in-the-loop control strategy presents yet another challenge.

Human during walking can sense the joint angle of the lower limb and the contact force exerted between the feet and the ground and uses such information as the feedback to regulate the impedance of the lower limb of a human. Thus, a human can achieve smooth switching between different walking speeds and adapts to various terrain conditions. In the previous works [14], [15], the leg prostheses are utilized to restore the motor of the lower limb. However, the active regulation of impedance cannot be fulfilled, and the amputees cannot actively conduct the impedance regulation and walk normally as a healthy human.

In fact, human gaits can be modeled as the Damping and Spring-Loaded Inverted Pendulum (D-SLIP) system [16], [17]. Although this D-SLIP could cause chaotic motions, impedance in the D-SLIP dynamics can lead to smooth switching among walking speeds, however, further evidence indicates that human motor control is primarily modulated by a complex relationship between proprioceptive sensation and joint movement. The human neuromusculoskeletal system is an extremely complex structure, with multiple degrees of freedom, sensory, and time delays during information transmission.

Nevertheless, humans can perform movements easily by relying on the incorporation of feedback and feedforward control [18]. The defined motor task can be addressed by using the motor commands, which are produced based on the implicit or explicit models of the body and the environment [19]. The uncertainties existing in the model can be compensated by tuning the feedforward control with the feedback. To acquire and maintain the feedforward control models [20], [21], the feedback is of vital importance. The mechanisms of the human motor control system should be replicated when a natural limb is replaced with an artificial one. The control loop from the sensory information of the prosthesis to the joint movement needs to be closed, forming human-in-the-loop control of the robotic leg prostheses.

In this work, we develop noninvasive FES (nFES) channels to reproduce the sensory feedback to facilitate the motion control of the robotic leg prosthesis. The proprioceptive sensation has been restored to sense the joint movement and the amount of force exerted on the ground.

By developing the model between the restored sensory feedback and the active regulation of the impedance of the leg prosthesis, the impedance of the active leg prosthesis can be successfully regulated according to the restored sensory feedback using several amputees equipped with our developed prosthesis. The amputee with the active leg prosthesis can smoothly switch between different walking speeds and adapt to various terrain conditions.

The experimental testing shows that this noninvasive sensory feedback can accurately sense the environment and, together with the inherent controller, form a human-in-the-loop control system to improve amputee mobility.

II. Model

A. Restoration of Sensory Feedback

Fig. 1 shows the participant restoration of the sensory feedback system with four noninvasive electrodes on the stump of the amputee. Fig. 1(a) shows the transversal surface of the stump of the amputee. Fig. 1(b) shows the vertical view of the stump of the amputee. Fig. 1(c) shows the lateral view of the position of electrodes to induce the sense of knee joint movement. Fig. 1(d) shows the position of electrodes to induce the sense of torque M_x, torque M_y, and the knee joint movement.

In order to induce sensation in the amputee, the muscles were activated by electrical stimulation via four electrodes placed around the stump of the subject. The placement was determined based on how well their positions were related to the force on the footplate and the knee movement of the leg prosthesis. The four-electrode array allows the selection of different pairs to be used during stimulation. The various pairs produced diverse electrical fields that different groups of muscles in the stump can be activated leading to sensations produced in different regions [22], [23].

Since the knee joint can only bend to the back of the leg, the electrode FES1 is placed on the back of the subject's stump, as

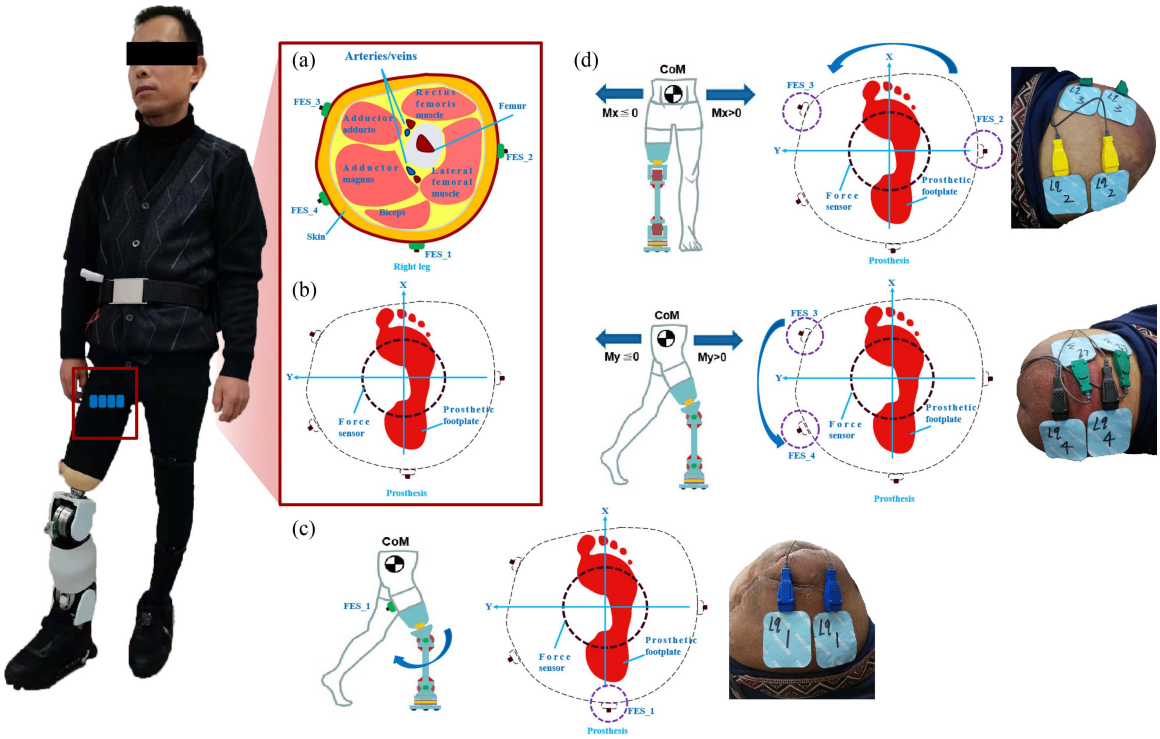

Fig. 1. Restoration of sensory feedback. (a) Transversal surface of the stump of the amputee. (b) Vertical view of the stump of the amputee. (c) Lateral view for the position of electrodes to induce the sense of knee joint movement. (d) Position of electrodes to induce the sense of torque M_x, torque M_y, and the knee joint movement.

shown in Fig. 1(c). When the knee joint of the leg prosthesis bends backward, the electrode FES1 stimulates the muscle tissue to induce the subject's proprioception for the knee joint movement of the leg prosthesis. The electrode FES2 is placed on the right of the subject's stump, as shown in Fig. 1(d). When the center of mass (CoM) of the subject has been transferred to the right of the leg prosthesis, M_x from the force sensor at the ankle joint of the leg prosthesis will have $M_x \leq 0$. The electrode FES2 stimulates the muscle tissue to induce the subject's proprioception for the change of M_x to sense the right movement of the subject. The electrode FES3 is placed on the left front of the subject's stump, as shown in Fig. 1(d). When the CoM of the subject has been transferred to the left front of the leg prosthesis, M_x and M_y from the force sensor will have $M_x > 0$, $M_y > 0$. The electrode FES3 stimulates the muscle tissue to induce the subject's proprioception for the change of M_x and M_y to sense the left front movement of the subject. The electrode FES4 is placed on the left rear of the subject's stump, as shown in Fig. 1(d). When CoM of the subject has been transferred to the left rear of the leg prosthesis, M_y from the force sensor will have $M_y \leq 0$. The electrode FES4 stimulates the muscle tissue to induce the subject's proprioception for the change of M_y to sense the left rear movement of the subject. The positions of the electrodes are different for each user, to activate the same group of muscles on the different position of the stump.

The relationship between joint movement and the electrode's behavior has been modeled as $\Gamma_{\text{sense}} = [T_{\text{touch-down}}, T_{\text{leave-off}}, h_{\text{obstacle}}]^T = H[\text{FES1}, \text{FES2}, \text{FES3}, \text{FES4}]^T$. Γ_{sense} represents the restored sensation, where $T_{\text{touch-down}}$ represents the sense for the touch-down moment of the prosthesis, $T_{\text{leave-off}}$ represents the sense for the leave-off moment of the prosthesis, and h_{obstacle} represents the sense for the height of small obstacles on the ground. $H \in \mathbb{R}^{3\times4}$ is a constant matrix. FES1, FES2, FES3, and FES4 represent the stimulating current for electrodes, where $\text{FES1} = \kappa_{\text{FES1}} \cdot q_{\text{knee}}$, κ_{FES1} is a constant value, $\text{FES2} = M_x$, when $M_x \leq 0$, $\text{FES3} = \max(M_x, M_y)$, when $M_x > 0$, and $M_y > 0$, and $\text{FES4} = M_y$, when $M_y \leq 0$.

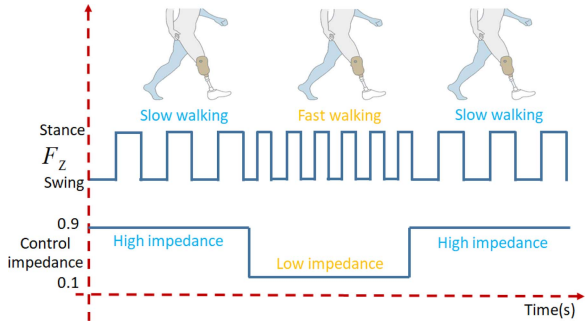

Fig. 2. Details of the unified gait generator's implementation.

B. Unified Gait Generator

The details of the unified gait generator's implementation are shown in Fig. 2. First, the value of F_z has been analyzed to

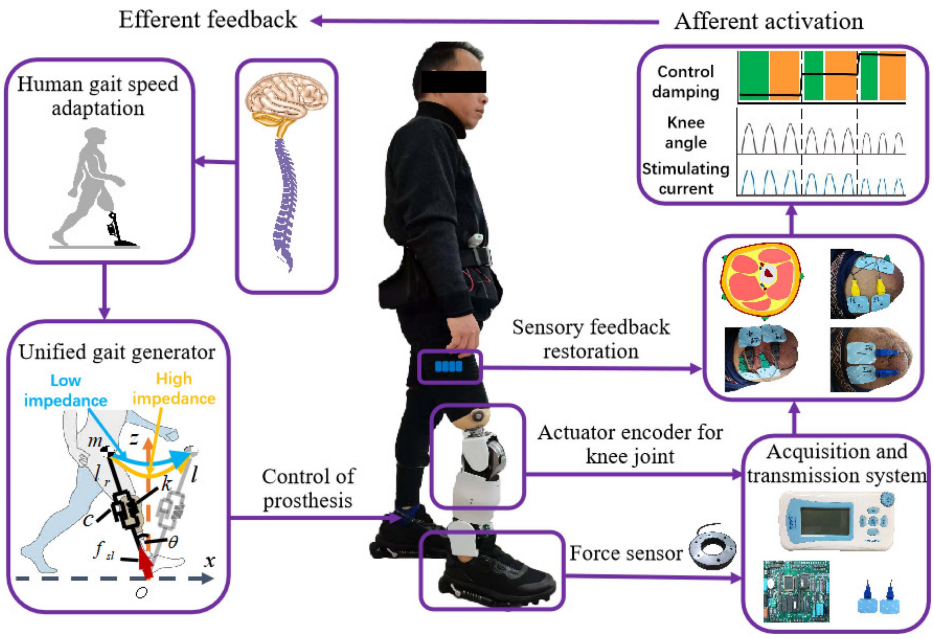

Fig. 3. Overview of the human-in-the-loop control with the sensory feedback. This control method involves two parts: 1) the subject's intent was decoded and converted into the prosthesis' motor command; 2) the readout from prosthesis' sensors was sent back to the subject by nFES.

identify the walking phase of the leg prosthesis; then, the walking frequency of the subject can be calculated from the change of F_z; next, the impedance parameter of the leg prosthesis will be updated by the walking frequency of the subject, according to the D-SLIP model; finally, the walking gait can be generated from slow walking to fast walking, corresponding to the high impedance and the low impedance.

In fact, human walking can have high and low speeds. Humans change walking speeds by naturally selecting a gait speed to minimize the energy consumption of themselves. Walking is often modeled by an inverted pendulum model with straight legs [24], [25]. We employed a model that treats the center of gravity as a point mass connected with a pendulum with different impedances of the legs. According to the known walking model with internal impedance, the motor control can be designed by adjusting its internal impedance, and the transition motor can be easily achieved by changing the internal parameters, so that the internal variables can affect the transition motor automatically.

Many previous works have investigated the walking models to formulate the gait transition using the zero-moment point (ZMP) [26] for low-speed walking, and the SLIP method [27], [28] for high-speed walking. These extensions, unfortunately, are limited in modeling ZMP or SLIP-based gait because the gait features cannot be flexibly expressed. In contrast, the presented methods detailed in [29] and [30] effectively accomplished the transition of the biped locomotion from low speed to high speed by switching the internal parameters of its neural oscillators based on the central pattern generator. Therefore, such approaches can be centered on the brain model for locomotion, while others can overlook the dynamics of locomotion without its periodicity. Consequently, a novel gait generator needs to be developed to adequately represent the features of walking when considering the transition between different walking speeds.

As shown in Fig. 3, the dynamics of the human leg can be derived as follows:

$$\frac{d}{dt}(m\dot{l}) = ml\dot{\theta}^2 - mg\cos\theta + f_{sl} \tag{1}$$

$$f_{sl} = -k(l - l_r) - c\dot{l} \tag{2}$$

$$m\ddot{l} + c\dot{l} + (k - m\dot{\theta}^2)l = kl_r - mg\cos\theta \tag{3}$$

where l is the length of the human leg and can be measured as the distance from the contact point O between the leg and the ground to the CoM of the human body, θ is the angle between the leg l and the vertical direction z, k is the spring constant of the virtual spring, l_r is the rest length, c is the damping coefficient of the virtual damper, m denotes the mass of the human body, f_{sl} is the support force of the model generated by the virtual spring and damping forces, f_{sl} depends on the position control, and l_r is designed to maintain the system stability during walking.

In particular, the impedance, such as the combination parameter of k and c, is considered to be the gait parameter, which displays the features of walking with guaranteed periodic stability. As a result, the impedance ξ and the angular frequency ω_d can be utilized, and ω_d is related to the periodic stability.

Based on the natural angular frequency ω_0 and ξ, ω_d is defined as $\omega_d = \omega_0\sqrt{1-\xi^2}$, where $\omega_0 = \sqrt{\frac{k}{m}}$. Thus, k is a function of ξ defined as

$$k(\xi) = \frac{m\omega_d^2}{(1-\xi^2)} \tag{4}$$

where c is also a function of ξ defined as

$$c(\xi) = 2\xi\sqrt{mk(\xi)}. \tag{5}$$

As a result, ξ denotes the combination of k and c in terms of (4) and (5). Specifically, according to (3), the high and low ξ reflects stiff and compliant pendulums, representing the features of low gait speed walking and high gait speed walking, respectively. In this work, the D-SLIP model only considers $\xi \in (0, 1)$.

From the above approximation, the dynamics of the human leg can be represented to a second-order linear differential function

$$\ddot{l} + 2\hat{\xi}\hat{\omega}_0\dot{l} + \hat{\omega}_0^2 l = \frac{k}{\hat{m}} l_r - \frac{m}{\hat{m}} g\cos\theta \tag{6}$$

where $\hat{\omega}_0 = \sqrt{\hat{k}/\hat{m}}$, $\hat{\xi} = \hat{c}/(2\sqrt{\hat{m}\hat{k}})$, and $\hat{\omega}_d = \hat{\omega}_0\sqrt{1-\hat{\xi}^2}$. Note that $\hat{\xi} < 1$ was validated in the common variables setting. Therefore, the dynamics can be subsequently determined as follows:

$$l = e^{-\hat{\xi}\hat{\omega}_0 t}\left(A_1\cos\hat{\omega}_d t + A_2\sin\hat{\omega}_d t\right) + \frac{k}{\hat{k}} l_r - \frac{mg}{\sqrt{\hat{c}^2 + (\hat{k}-\hat{m})^2}}\cos\left(\theta \pm \alpha_g\right)$$

where A_1 and A_2 are set according to the initial states of each gait, and $\alpha_g = \tan^{-1}(\frac{\hat{c}}{\hat{k}-\hat{m}})$ is the phase difference.

In this article, we focus on the transition from the low gait speed walking to the high gait speed walking to investigate the performance of the unified gait generator with the sensory feedback under different walking conditions.

III. Control Method

A. Human-in-the-Loop Control of Robotic Leg Prosthesis

Human motor control relies on a combination of feedback and feedforward strategies. The aim of this study was to investigate artificial sensory feedback and human motor control in the context of walking with a prosthetic leg. Moreover, considering this combination of the sensory feedback and motor control strategies, humans can naturally switch between low and high gait speeds arbitrarily under a simple energy minimization principle.

The input to the prosthetic is the change of contacting force between the leg prosthesis and the ground. The user's intent can be registered by F_Z, which is the force along the vertical direction of the force sensor installed at the ankle joint of the leg prosthesis.

The structure of the human-in-the-loop control with the sensory feedback is shown in Fig. 3. In Fig. 3, the real-time human-in-the-loop control of a robotic leg prosthesis involves flexible decoding of the user's device command directly converted into a prosthesis motor command (efferent activation), and a simultaneous readout from the prosthesis sensors sent back to the user through noninvasive electronic stimulation (afferent feedback). The decoding of the motor command was performed by the unified gait generator, which was inspired by healthy human gait adaptation, and the encoding was simultaneously achieved by the noninvasive stimulation on the stump of the amputee.

The gait speed of a human can be modeled by the sensation of the leg contacting the ground as

$$\Upsilon_{\text{gait}} = \mu \cdot \Gamma_{\text{sense}} \tag{7}$$

where Υ_{gait} represents the walking speed of the amputee and μ represents the mapping factor from Γ_{sense} to Υ_{gait}.

The value of μ is determined by the subjective intention of the amputee. When μ is positive, the walking speed of the amputee is positively correlated with the restored sensation Γ_{sense}. The stronger the restored sensation Γ_{sense}, the faster the walking speed of the amputee. When μ is negative, the stronger the restored sensation Γ_{sense} and the slower the walking speed of the amputee. In fact, when the restored sensation Γ_{sense} is stronger, the amputees are more willing to increase their walking speed. Hence, μ is assumed to be a positive constant throughout the experiments.

Moreover, walking in different environments can produce different walking patterns, and the amputee has to regulate the walking patterns. Therefore, human cooperation control is necessary for encoding the motor command of the prosthesis and automatically producing the desired motor patterns of the amputee. In this article, a human-in-the-loop control has been proposed to regulate the walking patterns of the prosthesis according to the walking speed of the amputee. For example, the low speed leads to the slow walking pattern of the amputee while the high speed leads to the fast walking pattern of the amputee. However, the above control based on human gait speed adaptation cannot be achieved without restoring the proprioceptive sensation, e.g., sensing the joint movement and the force exerted on the ground, and encoding the prosthesis motor command for the amputee to control the prosthesis. According to these feedback information, the amputee can regulate his gait speeds for different walking patterns. Finally, by integrating the kinesthetic feedback, an amputee equipped with a robotic leg prosthesis can improve motion capability.

B. Controller

The free-body diagram of the leg prosthesis is shown in Fig. 4, and the dynamics of the leg prosthesis can be written as

$$M(q)\ddot{q} + C(q,\dot{q})\dot{q} + D\dot{q} + G(q) = \tau \tag{8}$$

where $q = [q_1, q_2]^T \in \mathbb{R}^2$ is the joint angular position, $M(q) \in \mathbb{R}^{2\times 2}$ is the inertia matrix, $M(q) = \begin{bmatrix} M_{11} & M_{12} \\ M_{21} & M_{22} \end{bmatrix}$, $M_{11} = m_1 d_1^2 + I_1 + I_2 + m_2(l_1^2 + d_2^2 + 2l_1 l_2\cos q_2)$, $M_{12} = m_2 d_2^2 + I_2 + m_2 l_2 d_2\cos q_2$, $M_{21} = m_2 d_2^2 + I_2 + m_2 l_2 d_2\cos q_2$, $M_{22} = m_2 d_2^2 + I_2$; $C(q,\dot{q}) \in \mathbb{R}^{2\times 2}$ is the centripetal-Coriolis matrix, $C(q,\dot{q}) = \begin{bmatrix} C_{11} & C_{12} \\ C_{21} & C_{22} \end{bmatrix}$, $C_{11} = -m_2 l_1 d_2\sin q_2\dot{q}_2$, $C_{12} = -m_2 l_1 d_2\sin q_2(\dot{q}_1 + \dot{q}_2)$, $C_{21} = m_2 l_1 d_2\sin q_2\dot{q}_1$, $C_{22} = 0$; $D\dot{q} \in \mathbb{R}^{2\times 2}$ is the viscous friction torque, $D = \begin{bmatrix} k_{v1} & 0 \\ 0 & k_{v2} \end{bmatrix}$; $G(q) \in \mathbb{R}^2$ is the gravitational torque, $G(q) = \begin{bmatrix} m_1 d_1 g\cos q_1 + m_2 g(d_2\cos(q_1+q_2) + l_1\cos q_1) \\ m_2 d_2 g\cos(q_1+q_2) \end{bmatrix}$; $\tau \in \mathbb{R}^2$

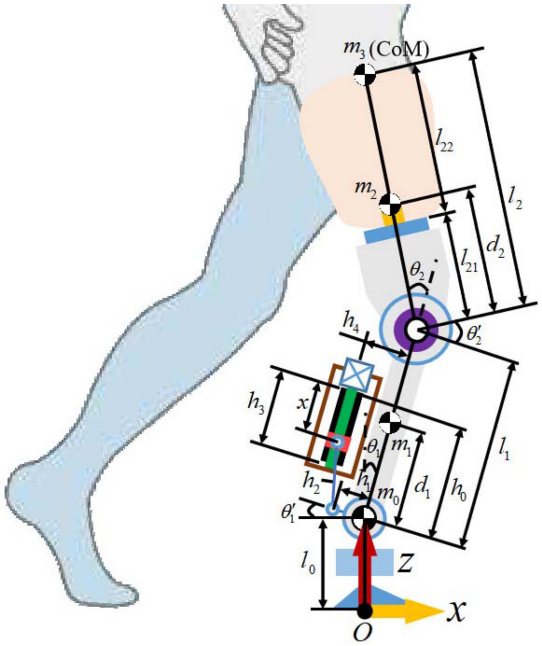

Fig. 4. Free body diagram of the leg prosthesis.

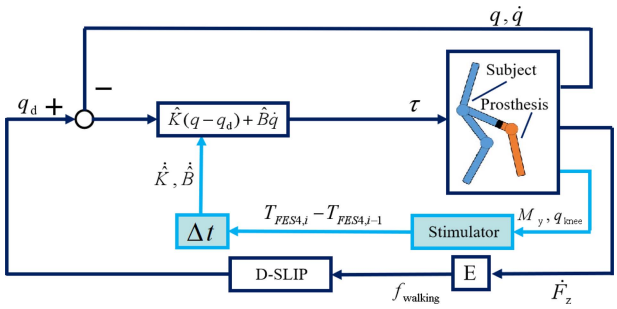

Fig. 5. Block diagram of the controller.

is the control torque. We denote that m_i is the mass of limb i, l_i is the length of limb i, l_{ci} is the distance from the limb joint to the centroid of limb i, I_i is the moment of inertia of limb i, k_{vi} is the coefficient of viscous friction of the joint i, g is the gravitational acceleration, and i=1, 2, i is the number of the limb of the leg prosthesis.

Let q_d=$[q_{d1}, q_{d2}]^T \in \mathbb{R}^2$ denote the desired output satisfying q_d, $\dot{q}_d$, $\ddot{q}_d \in L_\infty$.

The block diagram of controller is shown in Fig. 5. The control torque τ is designed as

$$\tau = \hat{K}\,(q - q_d) + \hat{B}\dot{q} \tag{9}$$

where q_d, q, and $\dot{q}$ represent the desired movement, the real movement, and the real velocity of joints of the prosthesis, respectively; $\dot{\hat{K}} = \begin{cases} r_K, & \Delta t \geq t_K \\ \frac{r_K}{t_K}\Delta t, & -t_K < \Delta t < t_K \\ -r_K, & \Delta t \leq -t_K \end{cases}$,

$\dot{\hat{B}} = \begin{cases} r_B, & \Delta t \geq t_B \\ \frac{r_B}{t_B}\Delta t, & -t_B < \Delta t < t_B \\ -r_B, & \Delta t \leq -t_B \end{cases}$, r_K, t_K, r_B, and t_B are positive constant values; $\Delta t = T_{\text{FES4},i} - T_{\text{FES4},i-1}$, can present the change of the touch-down moment of the leg prosthesis, $T_{\text{FES4},i}$ represents the current cycle time of FES4, $T_{\text{FES4},i-1}$ represents the previous cycle time of FES4; $\hat{K} = \begin{cases} K_{\text{up}}, & \hat{K} \geq K_{up} \\ \hat{K}, & K_{\text{down}} < \hat{K} < K_{\text{up}} \\ K_{\text{down}}, & 0 < \hat{K} \leq K_{\text{down}} \end{cases}$,

$\hat{B} = \begin{cases} B_{\text{up}}, & \hat{B} \geq B_{\text{up}} \\ \hat{B}, & B_{\text{down}} < \hat{B} < B_{\text{up}} \\ B_{\text{down}}, & 0 < \hat{B} \leq B_{\text{down}} \end{cases}$, K_{up}, K_{down}, B_{up}, and B_{down} are positive constant values; q_d is generated from the D-SLIP model, which has been regulated by f_{walking}; $f_{\text{walking}} = E\dot{F}_z$ represents the walking frequency of the subject, E is a constant value, and $\dot{F}_z$ represents the change frequency of F_z.

In fact, the human leg can be assumed as a virtual spring with spring constant k and damping coefficient c, in the previous works [16], [17], [30]. The support force f_{sl} of the leg can be modeled as $f_{sl} = -k(l - l_r) - c\dot{l}$, l_r represents the desired length of the leg, and l represents the real length of leg. $k = \frac{m\omega_d^2}{1-\xi^2}$, $c = 2\xi\sqrt{mk}$, m represents the mass of a human, ω_d represents the walking frequency, ξ represents the damping ratio of the leg. The high and low ξ, which represent a stiff and compliant leg, yield the characteristics of walking slowly and fast, respectively. When the walking is slow, ξ is high, k and c will be bigger, and the leg is stiff. When the walking is fast, ξ is low, k and c will be smaller, the leg is compliant.

C. Steady Analysis

The steady analysis of this control method can be guaranteed. When the sensory electrodes misfired, the subject can keep steady walking on the ground without shaking or falling.

As shown in Fig. 5, the stimulating current FES4 can regulate $\dot{\hat{K}}$ and $\dot{\hat{B}}$, to update $\hat{K}$ and $\hat{B}$. $\dot{\hat{K}}$ and $\dot{\hat{B}}$ are bounded by r_K and r_B, respectively. When the sensory electrodes misfired, $\hat{K}$ and $\hat{B}$ are bounded, and $\tau = \hat{K}(q - q_d) + \hat{B}\dot{q}$ is also bounded. As a result, the subject can keep steady walking on the ground without shaking or falling. Moreover, the desired walking gait q_d is generated from the D-SLIP model, having nothing to do with the sensory electrodes.

The stability in the context of the human–robot interaction is defined as the subject walks steadily on the ground without shaking or falling, and could start and stop freely.

The definition of periodic stability is as each joint of the leg prosthesis of the subject performs rhythmically according to a preset period. When the preset period is unchanged, the movements of each joint of the leg prosthesis will not change.

IV. Experiments and Results

A. Experiment Setup

Each experiment consists of two groups: 1) the group with the sensory feedback and 2) the group without the sensory feedback. All experimental results are analyzed at the presence or absence of sensory feedback.

TABLE I
MASS DISTRIBUTION OF ROBOTIC PROSTHESIS

Part	Mass(kg)	Weight	Configuration	Value
Body Structure	1.06	22%	Total Weight	4.8 kg
Ankle Motor Unit	0.91	19%	Height of Knee Joint	0.40 − 0.52 m
Knee Motor Unit	1.01	21%	Motion Range of Knee	0°−120°
Electronics Assembly	0.38	8%	Maximum Torque of Knee	80 N·m
Carbon Fiber Foot	0.86	18%	Motion Range of Ankle	−45° to 45°
Foot Shell	0.58	12%	Maximum Torque of Ankle	100 N·m
Total	4.8	100%		

TABLE II
PERFORMANCE OF DIFFERENT METHODS FOR ASSESSMENT OF SMALL OBSTACLE

Method	RMS(%)	MEAN(%)
Proposed method (with sensory feedback)	5.2	79.1
Existing method (without sensory feedback)	7.9	52.7

The objective of this article is to prove that the walking performance of the subject, such as walking speed, the ability to sense small obstacles on the ground, and so on, can be increased and improved by the restoration of the sensory feedback. The purpose of each task is not to regulate velocity but to quantify the improvement of walking performance after restoring the sensory feedback, such as the precision to sense the different heights of small obstacles, and the amount of increment for the walking speed and frequency on the level ground, *S* curve, or stairs.

Before each test, the subjects will learn the working principle of the FES feedback and have about 15 min of training time to familiarize themselves with the FES feedback.

1) Study Volunteers: The participants were recruited by a physician and evaluated by a psychologist prior to participating in the study. A 35-year-old and right-leg-dominant male with amputated for 5 years is selected as Subject 1, a 20-year-old and right-leg-dominant male with amputated for 2 years is chosen as Subject 2, a 40-year-old and right-leg-dominant male with amputated for 4 years is chosen as Subject 3, while a 22-year-old and right-leg-dominant male with amputated for 2 years is chosen as Subject 4. All procedures of this study were approved by the Ethics Committee of Yueyang Hospital of Integrated Traditional Chinese and Western Medicine, Shanghai University of Traditional Chinese Medicine. The registration number is ChiCTR2000031162, and the protocol number is 2019-014. All the subjects read and signed the informed consent.

2) Robotic Leg Prosthesis: Four noninvasive electrodes were placed on the stump of the subject. The robotic leg prosthesis consisting of 2-DOF powered joints was designed and optimized for the experiments in the USTC Robotic Laboratory [31]. The proposed robotic leg prosthesis is described as the structure planning, the sensor design, and the control system development. The mechanism of the prosthesis is created from 3-D printing through aluminum alloy and nylon fiber. The total mass of the robotic leg prosthesis is 4.8 kg, close to the healthy limb. Table I exhibits the prosthesis and the weight division. There are two active rotating joints operating the knee joint of the flexion about 120°, 1) the ankle joint of the dorsiflexion about 45° and 2) the planter flexion about −45°. The motor is the Maxon EC45 Powermax brushless for the leg joint. The length of the prosthesis depends on the coupler from the ball nut to the ankle and the pyramid connector, which couples the prosthesis to the socket of the subject. The data collected from the encoder and force sensors are used to evaluate its performance.

B. Assessment of Sensing the Height of Small Obstacle

To sense and judge the small obstacles is a key component of the human-in-the-loop control scheme. With the obstacle detection, the subject can sense small obstacles in time and judge the size of small obstacles more accurately. They can adjust their walking behavior in time, so as to avoid instability and even fall when stepping on small obstacles.

The prosthesis sensory feedback system allows the user to better sense the environment (e.g., small obstacles or uneven ground), so that the walking pattern can be adjusted to various ground conditions. Particularly, to test the ability of the sensory feedback, the considered test environment was scattered with small obstacles with height varying from 1.0 cm to 4.0 cm. During the test, the subjects were asked to determine the height of the obstacle on the ground. In each test trial, only one obstacle was selected and placed in the subject's walking direction. A total of 32 trials with different obstacle heights were performed and the subject walked forward without knowing the height of the obstacle.

As shown in Fig. 6, Fig. 6(a) denotes the four subjects' (Sub 1, Sub 2, Sub 3, and Sub 4) ability to accurately identify the height of small obstacles (1 cm, 2 cm, 3 cm, and 4 cm) with and without the sensory feedback. Actual heights for different obstacles are compared to the target height value for each subject. The line graph in Fig. 6(b) shows the degree of alignment with target identifying performance in this task shown in (a) for the four subjects (Sub 1, Sub 2, Sub 3, and Sub 4). The bar graph in Fig. 6(c) shows the average detection rate to self-generated error for the subjects at different obstacle heights. The results show that the subjects had a lower successful detection rate without the sensory feedback and that the sensory feedback increased the successful detection rate dramatically to more than 27% on average.

It is also found that the subjects showed an incredible learning speed in the use of the sensory feedback. As shown in Fig. 6(b), the deviation of the detected obstacle heights decreased when more test trials were performed.

Fig. 6(c) shows a decrease (except subject 1) in the performance of accurately identifying the small target. A possible explanation is that subjects (2, 3, and 4) cannot clearly figure

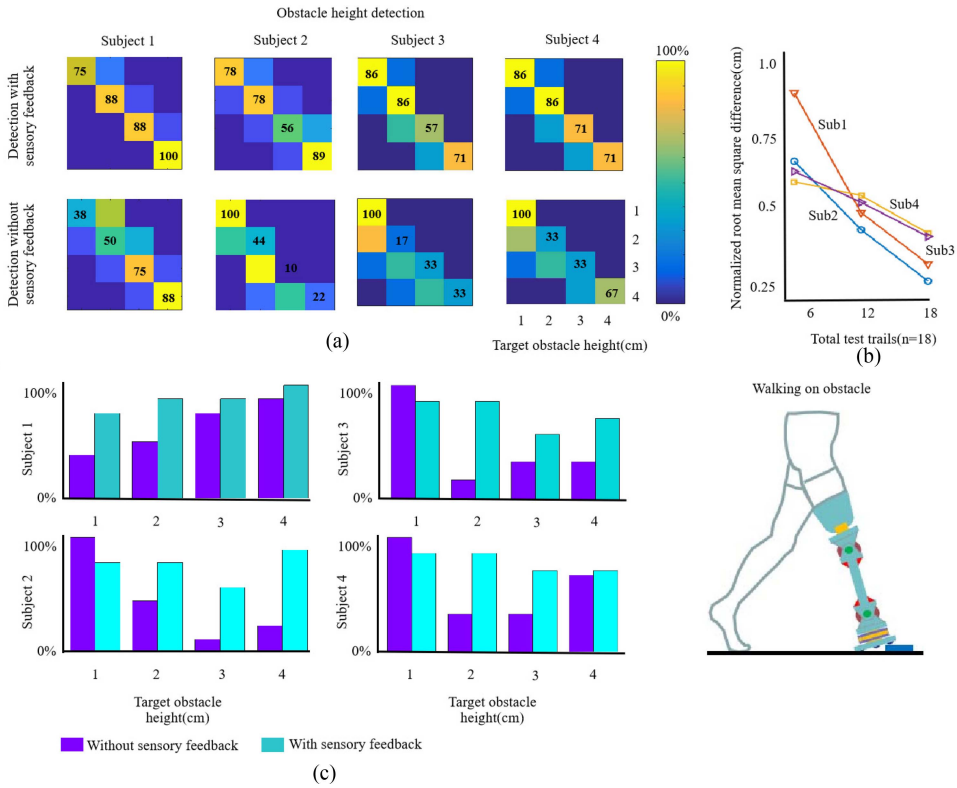

Fig. 6. Assessment of sensing the height of small obstacles. (a) Identification of the height of small obstacles (1 cm, 2 cm, 3 cm, and 4 cm) with and without the sensory feedback. (b) Line graph showing the degree of alignment with the target height of small obstacles. (c) Bar graph showing the average detection rate for different obstacles.

out the obstacles with a height of 1 cm and the other obstacles with different heights. When these subjects (2, 3, and 4) without the sensory feedback cannot feel the obvious change in the obstacle's height on the ground, they generally think that the height of this obstacle is 1 cm. That is why the detection rates of subjects (2, 3, and 4) without sensory feedback are almost 100% for the obstacle with a height of 1 cm, and the very low detection rates for other obstacles. When the subjects (1, 2, 3, and 4) are with the sensory feedback, they can clearly distinguish the obstacles with different heights, and the detection rates of obstacles with different heights begin to become more closer. The performance of different methods for the assessment of small obstacles is shown in Table II. In Table II, the proposed method has a smaller root-mean-square deviation and a higher average success rate, compared with the existing method without the sensory feedback.

C. Assessment of Walking Performance on Level Ground

In this experiment, the subjects were required to adopt different given walking speeds. For each trial, the subject was instructed to maintain the given walking speed, feel the motor, and sense the force reproduced by the stimulating electrodes. The subject walked at each given velocity for 18 trials. If the subject can control the velocity variation during the whole trial, this trial can be treated as a success, otherwise, it would be considered as a failure.

The target walking speed is not a fixed value. Before the trial, the subjects will be asked to walk according to three different target walking speeds without the sensory feedback, so the subjects will have an intuitive feeling of different target walking speeds. In the real trial, the subjects adjusted the walking speed according to their feelings. The trial can be treated as a success when the subject's walking speed was in the corresponding reference walking speed range, otherwise, it would be considered as a failure. Finally, the success rate of performance for each subject and all subjects can be calculated separately.

Fig. 7(a) shows the real-time motor control signal for the prosthetic leg, the ground reaction force, and the stimulating current injected in the stump. The sensing phase denotes the phase that the subject adapted to the desired walking velocity. The stable phase (shaded) denotes the phase that the subject maintained a desired stable walking velocity. Sensor readouts at three sites (knee joint angle, M_x, and M_y) were recorded and processed to induce the proprioceptive sensation. At the beginning of the test, the subjects' gait in the first few steps is messy. This stage is called the free phase. Then, the subjects began to adjust their walking speed, which is called the adaptive phase. Then, the subjects' walking speed was in a stable state, which was called the steady phase. At the end of the test, subjects began to slow down their walking speed, which is called the slow-down phase.

The walking capability of the subject greatly increased during a series of tests and training (as shown in Fig. 7(b), h denotes the high walking speed, m denotes the medium walking speed,

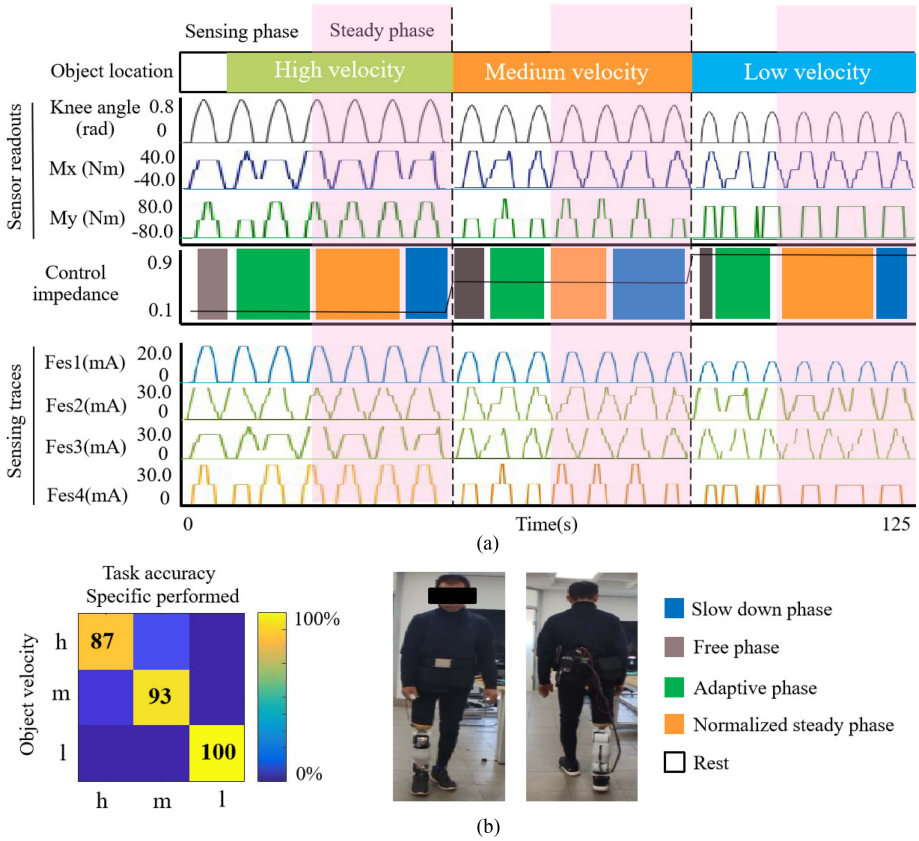

Fig. 7. Assessment of walking performance on level ground. (a) Sensor readouts at three sites (knee joint angle, M_x, and M_y) were recorded and processed to induce the proprioceptive sensation. (b) Confusion matrix indicates the success rate of walking performance on level ground (h for high, m for medium, and l for low).

TABLE III
PERFORMANCE OF DIFFERENT METHODS FOR ASSESSMENT OF WALKING ON LEVEL GROUND

Method	RMS(%)	MEAN(%)
Proposed method (with sensory feedback)	5.3	93.3
Existing method (without sensory feedback)	22.1	67

and l denotes the low walking speed), indicating that the subject recognized, through the sensory feedback, controlled the walking speed freely. The success of performing tasks increased from the group without the sensory feedback to the group with the sensory feedback from an initial 67% to 93.3%. This finding demonstrated that the subject had most likely undergone a learning process by integrating the restored sensation into human-in-the-loop control. The performance to achieve the desired walking speed's range for different methods on level ground is shown in Table III. In Table III, the proposed method has a smaller root-mean-square deviation and a higher average success rate, compared with the existing method without the sensory feedback.

D. Assessment of Walking Performance on S Curve and Stairs

In our daily life, people often walk along a curve or stairs. To evaluate how the proposed control method could adaptively handle various walking tasks, we tested the walking performance on the S curve and stairs. For each trial of the S curve walking, the subject was required to walk along the S curve (labeled on the ground) without a time limit. Each subject walked at three different velocities (0.8±0.1 m/s, 1.0±0.1 m/s, and 1.2±0.1 m/s) for 18 trials. The same experiment was conducted for climbing stairs at various velocities (0.7±0.1 m/s, 0.9±0.1 m/s, and 1.1±0.1 m/s).

As shown in Fig. 8, Fig. 8(a) shows the change of walking velocity and frequency on the S curve; Fig. 8(b) shows the change of walking velocity and frequency on stairs; Fig. 8(c) shows the confusion matrices of walking performance at different target walking velocities (h denotes the high walking speed, m denotes the medium walking speed, and l denotes the low walking speed). The target walking speeds used in the experiment are the walking speed usually used by the amputee in the daily life.

As shown in Fig. 8, the walking velocities at all three levels increased significantly when the human-in-the-loop control system was applied, and the average increments for low, medium, and high velocities in S curve walking were 0.23 m/s, 0.20 m/s, and 0.18 m/s, respectively. In climbing stairs, a similar increment was observed, from 0.75 m/s to 0.97 m/s for low velocity, from 0.8 m/s to 1.0 m/s for medium velocity, and from 0.85 m/s to 1.05 m/s for high velocity.

The increments of walking velocity and frequency are mainly due to our human-in-the-loop control, which helps the robotic

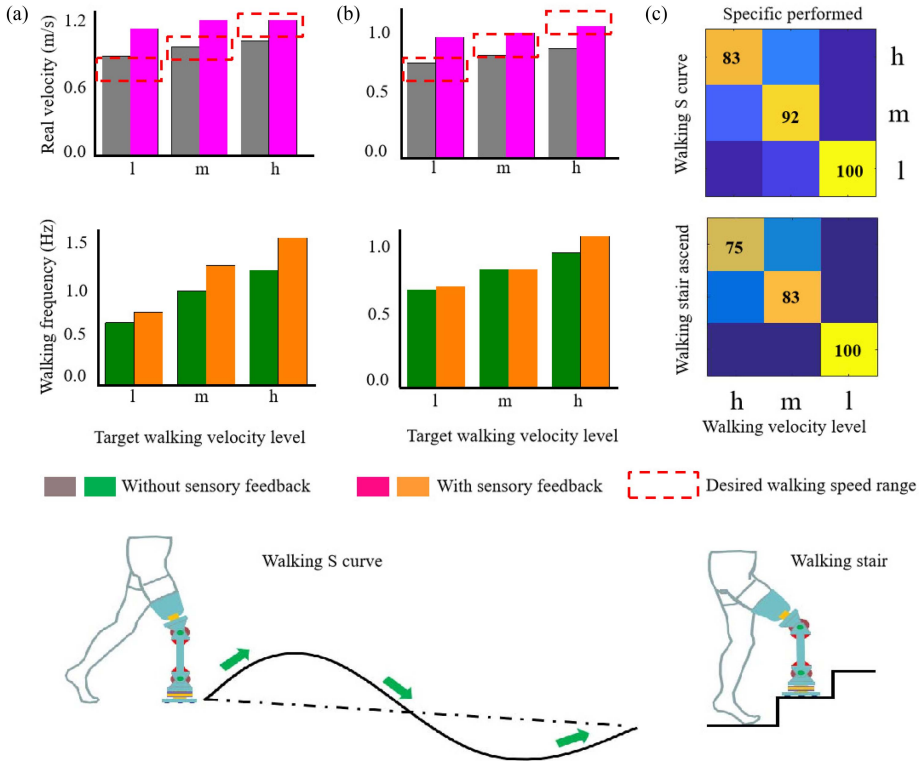

Fig. 8. Assessment of walking performance on the *S* curve and stairs. (a) Walking performance on the *S* curve. (b) Walking performance on stairs. (c) Confusion matrix indicates the success rate of walking performance on the *S* curve and stairs (*h* for high, *m* for medium, and *l* for low).

TABLE IV
PERFORMANCE OF DIFFERENT METHODS FOR ASSESSMENT OF WALKING ON *S* CURVE

Method	RMS(%)	MEAN(%)
Proposed method (with sensory feedback)	6.9	91.7
Existing method (without sensory feedback)	18.7	65

TABLE V
PERFORMANCE OF DIFFERENT METHODS FOR ASSESSMENT OF WALKING ON STAIRS ASCEND

Method	RMS(%)	MEAN(%)
Proposed method (with sensory feedback)	10.4	86
Existing method (without sensory feedback)	18.7	55

leg cooperate with the human to improve the walking behavior [see Fig. 8(c)]. The performance to achieve the desired walking speed's range for different methods on the *S* curve and stairs is shown in Tables IV and V. In Tables IV and V, the proposed method has a smaller root-mean-square deviation and a higher average success rate, compared with the existing method without the sensory feedback.

V. DISCUSSION

Despite recent advances in the development of lower-limb prosthetics, there are advantages restoring sensor feedback in controlling robotic leg prostheses for transtibial (below knee) or transfemoral (above knee) amputees. Most surgical invasive techniques to restore the sensory feedback are applied exclusively to transtibial amputations, a less severe clinical illness compared with transfemoral amputations. Upper-limb amputees, to perceive touch sensations from the lost hand and to exploit them for long-term prosthesis control, have been enabled by direct neuro-stimulation through transversal intrafascicular multichannel electrodes. However, merely a few cases with immediate nerve stimulation have been conducted, which did not present clear advantages for the leg amputees.

In this study, the sensory feedback was obtained from four noninvasive stimulation electrodes placed on the subject's stump. Using the sensory feedback, the subject adapted the walking speed according to the sense of the motor movement of the prosthesis and the contact condition between the prosthesis and the ground. When the subject walks on the level ground, the sensation of the touch between the prosthesis and the ground was enhanced by the noninvasive stimulation. The stimulating current was proportional to the contact force exerted from the ground. By sensing the change in the stimulating current, the subject was able to know the touch-down and leave-off moments. At the touch-down moment, the subject switched his walking gait to the support phase, and at the leave-off moment, the subject switched his walking gait to the swing phase.

VI. CONCLUSION

The challenges associated with limb loss not only include how to restore the lost proprioceptive sensation within prosthetic systems efficiently but also how to close the loop from the sensory feedback system to realize the normal human gait

adaptation efficiently. Inspired by human limb motor control and the human proprioception system, noninvasive electrical stimulation and a unified inherent controller were designed in this study. Significant improvement in the prosthesis motor control was identified with movement decoding and noninvasive stimulation sessions in the experiment.

REFERENCES

[1] S. Kontogiannopoulos, G. A. Bertos, and E. Papadopoulos, "'A biomechatronic EPP' upper-limb prosthesis control configuration and its performance comparison to other control configurations," *IEEE Trans. Med. Robot. Bionics*, vol. 2, no. 2, pp. 282–291, May 2020.

[2] D. R. Deo, P. Rezaii, L. R. Hochberg, A. M. Okamura, K. V. Shenoy, and J. M. Henderson, "Effects of peripheral haptic feedback on intracortical brain-computer interface control and associated sensory responses in motor cortex," *IEEE Trans. Haptics*, vol. 14, no. 4, pp. 762–775, Oct.–Dec. 2021.

[3] L. Vargas, H. Huang, Y. Zhu, and X. Hu, "Object recognition via evoked sensory feedback during control of a prosthetic hand," *IEEE Robot. Automat. Lett.*, vol. 7, no. 1, pp. 207–214, Jan. 2022.

[4] S. Raspopovic et al., "Restoring natural sensory feedback in real-time bidirectional hand prostheses," *Sci. Transl. Med.*, vol. 6, no. 222, 2014, Art. no. 222ra19.

[5] D. W. Tan et al., "A neural interface provides long-term stable natural contact perception," *Sci. Transl. Med.*, vol. 6, no. 257, 2014, Art. no. 257ra138.

[6] T. Tanabe, H. Yano, and H. Iwata, "Evaluation of the perceptual characteristics of a force induced by asymmetric vibrations," *IEEE Trans. Haptics*, vol. 11, no. 2, pp. 220–231, Apr.–Jun. 2018.

[7] T. A. Kuiken et al., "Targeted muscle reinnervation for real-time myoelectric control of multifunction artificial arms," *J. Amer. Med. Assoc.*, vol. 301, no. 6, pp. 619–628, 2009.

[8] T. A. Kung et al., "Regenerative peripheral nerve interface viability and signal transduction with an implanted electrode," *Plast. Reconstructive Surg.*, vol. 133, no. 6, pp. 1380–1394, 2014.

[9] Z. Li, W. Yuan, S. Zhao, Z. Yu, Y. Kang, and C. L. P. Chen, "Brain-actuated control of dual-arm robot manipulation with relative motion," *IEEE Trans. Cogn. Develop. Syst.*, vol. 11, no. 1, pp. 51–62, Mar. 2019.

[10] T. Alif, S. Bhasin, K. Garg, and D. Joshi, "An enhanced model free adaptive control approach for functional electrical stimulation assisted knee joint regulation and control," *IEEE Trans. Neural Syst. Rehabil. Eng.*, vol. 31, pp. 1584–1593, 2023.

[11] A. Shon, K. Brakel, M. Hook, and H. Park, "Closed-loop plantar cutaneous augmentation by electrical nerve stimulation increases ankle plantarflexion during treadmill walking," *IEEE Trans. Biomed. Eng.*, vol. 68, no. 9, pp. 2798–2809, Sep. 2021.

[12] S. Ren, W. Wang, Z.-G. Hou, X. Liang, J. Wang, and W. Shi, "Enhanced motor imagery based brain-computer interface via FES and VR for lower limbs," *IEEE Trans. Neural Syst. Rehabil. Eng.*, vol. 28, no. 8, pp. 1846–1855, Aug. 2020.

[13] S. Qiu et al., "Event-related beta EEG changes during active, passive movement and functional electrical stimulation of the lower limb," *IEEE Trans. Neural Syst. Rehabil. Eng.*, vol. 24, no. 2, pp. 283–290, Feb. 2016.

[14] F. M. Petrini et al., "Enhancing functional abilities and cognitive integration of the lower limb prosthesis," *Sci. Transl. Med.*, vol. 11, no. 512, 2019, Art. no. eaav8939.

[15] F. M. Petrini et al., "Sensory feedback restoration in leg amputees improves walking speed, metabolic cost and phantom pain," *Nature Med.*, vol. 25, pp. 1356–1363, 2019.

[16] T. Kobayashi et al., "Unified bipedal gait for autonomous transition between walking and running in pursuit of energy minimization," *Robot. Auton. Syst.*, vol. 103, pp. 27–41, 2018.

[17] H. Geyer, A. Seyfarth, and R. Blickhan, "Compliant leg behaviour explains basic dynamics of walking and running," *Proc. Roy. Soc. London Ser. B*, vol. 273, pp. 2861–2867, 2006.

[18] D. W. Franklin and D. M. Wolpert, "Computational mechanisms of sensorimotor control," *Neuron*, vol. 72, no. 3, pp. 425–442, 2011.

[19] M. C. Capolei, N. A. Andersen, H. H. Lund, E. Falotico, and S. Tolu, "A cerebellar internal models control architecture for online sensorimotor adaptation of a humanoid robot acting in a dynamic environment," *IEEE Robot. Autom. Lett.*, vol. 5, no. 1, pp. 80–87, Jan. 2020.

[20] A. Accetta, M. Cirrincione, F. D'Ippolito, M. Pucci, and A. Sferlazza, "Adaptive feedback linearization control of SynRM drives with online inductance estimation," *IEEE Trans. Ind. Appl.*, vol. 59, no. 2, pp. 1824–1835, Mar./Apr. 2023.

[21] J. Cheng, Y. Wang, J. H. Park, J. Cao, and K. Shi, "Static output feedback quantized control for fuzzy Markovian switching singularly perturbed systems with deception attacks," *IEEE Trans. Fuzzy Syst.*, vol. 30, no. 4, pp. 1036–1047, Apr. 2022.

[22] L. Vargas, H. Huang, Y. Zhu, and X. Hu, "Merged haptic sensation in the hand during concurrent non-invasive proximal nerve stimulation," in *Proc. IEEE 40th Annu. Int. Conf. Eng. Med. Biol. Soc.*, 2018, pp. 2186–2189.

[23] L. Vargas, H. Huang, Y. Zhu, and X. Hu, "Stiffness perception using transcutaneous electrical stimulation during active and passive prosthetic control," in *Proc. IEEE 42nd Annu. Int. Conf. Eng. Med. Biol. Soc.*, 2020, pp. 3909–3912.

[24] L. Li, I. Tokuda, and F. Asano, "Energy-efficient locomotion generation and theoretical analysis of a quasi-passive dynamic walker," *IEEE Robot. Autom. Lett.*, vol. 5, no. 3, pp. 4305–4312, Jul. 2020.

[25] H. Y. Park, J. H. Kim, and K. Yamamoto, "A new stability framework for trajectory tracking control of biped walking robots," *IEEE Trans. Ind. Informat.*, vol. 18, no. 10, pp. 6767–6777, Oct. 2022.

[26] J. H. Kim, J. Lee, and Y. Oh, "A theoretical framework for stability regions for standing balance of humanoids based on their LIPM treatment," *IEEE Trans. Syst., Man, Cybern. Syst.*, vol. 50, no. 11, pp. 4569–4586, Nov. 2020.

[27] X. Xiong and A. D. Ames, "Dynamic and versatile humanoid walking via embedding 3D actuated SLIP model with hybrid LIP based stepping," *IEEE Robot. Automat. Lett.*, vol. 5, no. 4, pp. 6286–6293, Oct. 2020.

[28] X. Xiong and A. Ames, "SLIP walking over rough terrain via H-LIP stepping and backstepping-barrier function inspired quadratic program," *IEEE Robot. Automat. Lett.*, vol. 6, no. 2, pp. 2122–2129, Apr. 2021.

[29] C. Liu, D. Wang, and Q. Chen, "Central pattern generator inspired control for adaptive walking of biped robots," *IEEE Trans. Syst., Man, Cybern. Syst.*, vol. 43, no. 5, pp. 1206–1215, Sep. 2013.

[30] U. I. Khan and Z. Chen, "Natural oscillation gait in humanoid biped locomotion," *IEEE Trans. Control Syst. Technol.*, vol. 28, no. 6, pp. 2309–2321, Nov. 2020.

[31] M. Pi et al., "Biologically inspired deadbeat control of robotic leg prostheses," *IEEE Trans. Mechatronics*, vol. 25, no. 6, pp. 2733–2742, Dec. 2020.

Ming Pi received the Ph.D. degree in automation from the University of Science and Technology of China, Hefei, China, in 2021.

He is currently a Lecturer with the School of Information Engineering, Southwest University of Science and Technology, Mianyang, China. His current research interests include the bionic robot control and the special environment robot control.

Zhijun Li (Fellow, IEEE) received the Ph.D. degree in mechatronics from Shanghai Jiao Tong University, Shanghai, China, in 2002.

From 2003 to 2005, he was a Postdoctoral Fellow with the Department of Mechanical Engineering and Intelligent Systems, The University of Electro-Communications, Tokyo, Japan. From 2005 to 2006, he was a Research Fellow with the Department of Electrical and Computer Engineering, National University of Singapore, and Nanyang Technological University, Singapore. He is currently a Chair Professor with Tongji University, Shanghai. His current research interests include wearable robotics and biomechatronics systems.

Dr. Li has been the Co-Chair of the IEEE SMC Technical Committee on Biomechatronics and Biorobotics Systems (B^2S) and the IEEE RAS Technical Committee on Neuro-Robotics Systems since 2016. He is an AAIA Fellow. He is a Member of the Board of Governors, IEEE Systems, Man, and Cybernetics Society from 2023 to 2025.

Qinjian Li received the B.S. degree in automation from the Nanjing Institute of Technology, Nanjing, China, in 2015. He is currently working toward the Ph.D. degree in automation with the University of Science and Technology of China, Hefei, China.

His current research interests include design, simulation, and control of robotic leg prostheses.

Yu Kang (Senior Member, IEEE) received the Dr.Eng. degree in control theory and control engineering from the University of Science and Technology of China, Hefei, China, in 2005.

From 2005 to 2007, he was a Postdoctoral Fellow with the Academy of Mathematics and Systems Science, Chinese Academy of Sciences, Beijing, China. He is currently a Professor with the Department of Automation, with the State Key Laboratory of Fire Science, and with the Institute of Advanced Technology, University of Science and Technology of China. His current research interests include adaptive/robust control, variable structure control, mobile manipulators, and Markovian jump systems.

Zhen Kan (Senior Member, IEEE) received the Ph.D. degree in mechanical and aerospace engineering from the University of Florida, Gainesville, FL, USA, in 2011.

He was a Postdoctoral Research Fellow with Air Force Research Laboratory, Eglin AFB, FL, USA, and the University of Florida REEF, Shalimar, FL, USA, from 2012 to 2016, and an Assistant Professor with the Department of Mechanical Engineering, University of Iowa, Iowa City, IA, USA. He is currently a Professor with the Department of Automation, University of Science and Technology of China, Hefei, China. His current research interests include networked robotic systems, Lyapunov-based nonlinear control, graph theory, complex networks, human-assisted estimation, planning, and decision making.

Dr. Kan is currently an Associate Editor with the Conference Editorial Board of IEEE Control Systems Society and Technical Committee for several internationally recognized scientific and engineering conferences.

Rong Song (Senior Member, IEEE) received the B.Eng. degree in electrical engineering from Tsinghua University, Beijing, China, in 1999, the M.S. degree in electronic engineering from Shantou University, Shantou, China, in 2002, and the Ph.D. degree in biomedical engineering from Hong Kong Polytechnic University, Hong Kong, in 2006.

He is currently a Professor with the School of Biomedical Engineering, Sun Yat-sen University, Guangzhou, China. His research interests include musculoskeletal modeling, biomedical signal processing, human motion analysis, robot-assisted stroke rehabilitation, human–robot interaction, biomedical signal processing, and rehabilitation evaluation.